JVI Journals.ASM.org

Brain Invasion by Mouse Hepatitis Virus Depends on Impairment of Tight Junctions and Beta Interferon Production in Brain Microvascular Endothelial Cells

Christian Bleau,[a] Aveline Filliol,[b] Michel Samson,[b] Lucie Lamontagne[a]

Département des Sciences Biologiques, Université du Québec à Montréal, Montréal, Québec, Canada[a]; Institut de Recherche en Santé-Environnement-Travail, Université de Rennes 1, Rennes, France[b]

ABSTRACT

Coronaviruses (CoVs) have shown neuroinvasive properties in humans and animals secondary to replication in peripheral organs, but the mechanism of neuroinvasion is unknown. The major aim of our work was to evaluate the ability of CoVs to enter the central nervous system (CNS) through the blood-brain barrier (BBB). Using the highly hepatotropic mouse hepatitis virus type 3 (MHV3), its attenuated variant, 51.6-MHV3, which shows low tropism for endothelial cells, and the weakly hepatotropic MHV-A59 strain from the murine coronavirus group, we investigated the virus-induced dysfunctions of BBB *in vivo* and in brain microvascular endothelial cells (BMECs) *in vitro*. We report here a MHV strain-specific ability to cross the BBB during acute infection according to their virulence for liver. Brain invasion was observed only in MHV3-infected mice and correlated with enhanced BBB permeability associated with decreased expression of zona occludens protein 1 (ZO-1), VE-cadherin, and occludin, but not claudin-5, in the brain or in cultured BMECs. BBB breakdown in MHV3 infection was not related to production of barrier-dysregulating inflammatory cytokines or chemokines by infected BMECs but rather to a downregulation of barrier protective beta interferon (IFN-β) production. Our findings highlight the importance of IFN-β production by infected BMECs in preserving BBB function and preventing access of blood-borne infectious viruses to the brain.

IMPORTANCE

Coronaviruses (CoVs) infect several mammals, including humans, and are associated with respiratory, gastrointestinal, and/or neurological diseases. There is some evidence that suggest that human respiratory CoVs may show neuroinvasive properties. Indeed, the severe acute respiratory syndrome coronavirus (SARS-CoV), causing severe acute respiratory syndrome, and the CoVs OC43 and 229E were found in the brains of SARS patients and multiple sclerosis patients, respectively. These findings suggest that hematogenously spread CoVs may gain access to the CNS at the BBB level. Herein we report for the first time that CoVs exhibit the ability to cross the BBB according to strain virulence. BBB invasion by CoVs correlates with virus-induced disruption of tight junctions on BMECs, leading to BBB dysfunction and enhanced permeability. We provide evidence that production of IFN-β by BMECs during CoV infection may prevent BBB breakdown and brain viral invasion.

The blood-brain barrier (BBB) is a highly selective barrier critical for central nervous system (CNS) homeostasis in controlling peripheral blood-brain exchange and preventing neurotoxins and pathogens from access to the CNS. The functional and structural integrity of the BBB mainly relies on specific features of the brain microvascular endothelial cells (BMECs) lining the brain capillaries. These cells are tightly connected by a unique assembly of adherens junctions composed of transmembrane cadherin and tight-junction complexes (e.g., claudins and occludin) anchored to actin filaments via adaptor molecules, such as zona occludens (ZO) (1).

The BBB is known to provide significant protection against hematogenously spread viruses, as several viruses inoculated in periphery were shown to induce neuropathology only after mechanically or chemically mediated disruption of the BBB (2–4). However, some infectious blood-borne viruses primarily targeting peripheral organs have evolved strategies to thwart the BBB, including direct infection of BMECs, "Trojan horse" invasion via the traffic of infected immune cells in the CNS or paracellular entry through alteration of tight junctions (1). Disruption of tight junctions, resulting from either viral products or host immune factors (5–8), may lead to an increase in extravasation of immune cells and poorly regulated flux of molecules as well as ions across the BBB, which are critical events in neuropathogenesis (9).

Coronaviruses (CoVs) are enveloped, positive-sense, single-stranded RNA viruses that infect several mammals, including humans. There is some evidence that suggests that respiratory CoVs may show neuroinvasive properties. The severe acute respiratory syndrome coronavirus (SARS-CoV), which causes severe acute respiratory syndrome in humans, and the human CoVs OC43 and 229E were found in the brains of SARS patients and multiple scle-

Received 9 June 2015 **Accepted** 13 July 2015

Accepted manuscript posted online 22 July 2015

Citation Bleau C, Filliol A, Samson M, Lamontagne L. 2015. Brain invasion by mouse hepatitis virus depends on impairment of tight junctions and beta interferon production in brain microvascular endothelial cells. J Virol 89:9896–9908. doi:10.1128/JVI.01501-15.

Editor: S. Perlman

Address correspondence to Lucie Lamontagne, lamontagne.lucie@uqam.ca.

doi:10.1128/JVI.01501-15

rosis patients, respectively (10–13). However, the mechanism of neuroinvasion by hematogenously spread CoVs is elusive.

The different serotypes of viruses in the mouse hepatitis virus (MHV) coronavirus group induce hepatic, respiratory, or enteric diseases, followed by neurological disorders (14), and thus, the mouse is a relevant animal model for the study of neuroinvasion by CoVs. The highly hepatotropic mouse hepatitis virus type 3 (MHV3) is known as the most virulent MHV strain, causing fulminant hepatitis and death of susceptible C57BL/6 mice within 3 to 5 days postinfection (p.i.) (15) and neurological disease following nonlethal hepatitis in semisusceptible C3H mice characterized by meningitis, ependymitis, and encephalitis beginning 3 to 4 weeks p.i. after intraperitoneal (i.p.) infection (15, 16). This suggests brain invasion by MHV3 through the BBB endothelium in the acute phase of infection. The attenuated 51.6-MHV3 variant has lost the ability to replicate in liver endothelial cells (17) and induces acute hepatitis and death of susceptible C57BL/6 mice within 5 to 9 days p.i. (18), suggesting an important role for endothelial cells in disease outcome. The weakly hepatotropic MHV-A59 causes no mortality and moderate hepatitis without neurological disease in C57BL/6 mice when i.p. inoculated (19). Brain invasion and disease by the MHV-A59 serotype is however enabled following intranasal infection and depends on the olfactory nerve, instead of the BBB, as the portal of viral entry into the CNS (19–21) suggesting a restriction of CNS invasion at the BBB level (19, 22).

BMECs have already been reported as potential cell targets for MHVs, as they express the MHV receptor, carcinoembryonic antigen 1a (CEACAM1a) (23). Primary mouse BMECs were shown to support MHV3 replication *in vitro* (24), but conflicting results regarding viral replication of MHV-A59 in BMECs have been reported (22, 25, 26). Since all MHV strains use the same cell receptor (CEACAM1a), and both MHV3 and MHV-A59 can bind to BMECs (22, 24), another factor(s) might be involved in BBB invasion according to MHV serotype.

We demonstrated here that the highly hepatotropic MHV3 strain, but not the MHV-A59 or 51.6-MHV3 variant, elicited an *in vivo* and *in vitro* breakdown of functional and structural integrity of the BBB, enabling viral invasion of the brain. The MHV strain-specific ability to cross the BBB during acute liver infection correlated with enhanced BBB permeability due to alteration of tight junctions zona occludens protein 1 (ZO-1), VE-cadherin, and occludin but not claudin-5 expression on BMECs. Barrier disruption in MHV3 infection was not related to the release of inflammatory cytokines or chemokines by infected BMECs but rather to a downregulation of barrier protective beta interferon (IFN-β) production.

MATERIALS AND METHODS

Mice. Female C57BL/6 (Charles River, St. Constant, Quebec, Canada) mice were housed in a HEPA-filtered air environment. All experiments were conducted with mice between 8 to 10 weeks of age in compliance with the regulations of the Animal Committee of the University of Quebec at Montreal, Canada.

Viruses. Highly pathogenic MHV3 is a cloned substrain isolated from the liver of an infected DBA2 mouse and maintained in L2 cells for less than three passages, as described previously (27). The mildly virulent MHV-A59 strain was obtained from the American Type Culture Collection (ATCC) (Rockville, MD, USA). The lower-virulence 51.6-MHV3 is an escape mutant, selected from the pathogenic MHV3 virus in the presence of S protein-specific A51 and A37 monoclonal antibodies, having lost tropism for liver sinusoidal endothelial cells (17). All viruses were produced in L2 cells, and their pathogenic properties were assessed routinely.

Cells. bEnd.3 (ATCC CRL-2390), an immortalized mouse brain endothelial cell line, was cultured in RPMI 1640 medium supplemented with 10% heat-inactivated fetal calf serum (FCS) and antibiotics (Wysent, St. Bruno, Quebec, Canada). Freshly trypsinized bEnd.3 cells were seeded in collagen-treated 24-well plates at 6×10^4 cells/cm^2 or collagen-treated 6.5-mm-diameter Transwell polycarbonate membrane inserts (Fisher Scientific, Ontario, Canada) and incubated until they reached confluence. The cells were then infected with MHV3, MHV-A59, or 51.6-MHV3 at a multiplicity of infection (MOI) of 0.1 for 24 to 72 h or up to 8 days according to the particular experiment. In some experiments, cells were concomitantly treated with IFN-β (100 pg/ml) or anti-IFN-β (1 μg/ml) (R&D Systems, Minneapolis, MN). Cell culture supernatant was collected for enzyme-linked immunosorbent assays (ELISAs) and virus titration, and total RNA was extracted for quantitative reverse transcription-PCR (qRT-PCR) analyses. *In vitro* studies were conducted in triplicate.

***In vivo* viral infections.** Groups of six wild-type C57BL/6 mice were infected intraperitoneally (i.p.) with 10^3 50% tissue culture infective doses ($TCID_{50}$) of MHV3, MHV-A59, or 51.6-MHV3. Mock-infected mice received a similar volume of phosphate-buffered saline (PBS) (Wysent, St. Bruno, Quebec, Canada). Mice were sacrificed by CO_2 anoxia 72 h postinfection (p.i.). The brain and liver were collected and frozen at −80°C for further analyses.

RNA isolation and qRT-PCR. Total RNA from frozen brain samples was extracted using TRIzol reagent (Invitrogen, Burlington, Ontario, Canada), and residual genomic DNA was removed with the Turbo DNA-free kit (Ambion, Austin, TX). RNA from bEnd.3 cells was extracted using a NucleoSpin RNA II kit (Macherey-Nagel, Bethlehem, PA) according to the manufacturer's instructions. One microgram of RNA was reverse transcribed into cDNA using the high-capacity cDNA reverse transcription kit (Applied Biosystems, Foster City, CA). Real-time PCR amplification was carried out on 25 ng cDNA using the HotStart-IT SYBR green qPCR master mix (USB Corporation, Cleveland, OH) on an ABI 7300 system (Applied Biosystems, Foster City, CA). Primer sets used are listed in Table 1. Threshold cycle (C_T) values were collected and used for $\Delta\Delta C_T$ analysis. Gene expression was normalized to expression of the hypoxanthine phosphoribosyltransferase (HPRT) gene as an endogenous control and expressed as a ratio of gene expression in mock-infected mice or bEnd.3 cells. The specificity of the PCR products was confirmed by melting curve analyses. All qPCR analyses of samples from *in vitro* and *in vivo* experiments were run in duplicate.

ELISAs. Determination of the levels of IFN-β (PBL, Piscataway, NJ), interleukin 6 (IL-6), tumor necrosis factor alpha (TNF-α) (BD, Mississauga, Ontario, Canada), CXC chemokine ligand 10 (CXCL10), CC chemokine ligand 2 (CCL2) (eBiosciences, San Diego, CA), and CXCL1 (R&D Systems, Minneapolis, MN) in bEnd.3 cell culture supernatants was carried out according to the manufacturer's instructions.

Virus titration. Virus titration was performed on brain lysates from infected mice and infected bEnd.3 cell culture supernatants by 10-fold serial dilutions on L2 cell monolayers cultured in 96-well plates. Cytopathic effects, characterized by syncytia and cell lysis, were recorded at 72 h p.i., and virus titers were determined according to the Reed-Muench method and expressed as $\log_{10}$ $TCID_{50}$.

***In vivo* assessment of BBB integrity.** Changes in blood-brain barrier permeability were assessed using sodium fluorescein (NaF) (Sigma-Aldrich) as previously described (28). Briefly, mice were infected for 72 h and i.p. injected with 100 μl of 10% NaF in PBS 1 h prior to euthanasia. Cardiac blood was collected, transcardial perfusion with 15 ml PBS was performed, and brains were removed, weighed, and homogenized in PBS (1:10 [wt/vol]). NaF content was measured on a Synergy 4 microplate fluorometer (Biotek, Winooski, VT) with excitation at 485 nm and emission at 530 nm using standards ranging from 0.78 μg/ml to 5 μg/ml. The NaF concentration in the brain was normalized to serum NaF concentrations for each mouse to allow comparisons among mice and calculated as

TABLE 1 Primer sets used for quantitative reverse transcription-PCR

Gene	Primer sequence	
	Forward primer	Reverse primer
HPRT	5′-GAAAGACTTGCTCGAGATGTCATG-3′	5′-CACACAGAGGGCCACAATGT-3′
IFN-β	5′-CGGACTTCAAGATCCCTATGGA-3′	5′-TGGCAAAGGCAGTGTAACTCTTC-3′
IL-6	5′-TCGGAGGCTTAATTACACATGTTC-3′	5′-TGCCATTGCACAACTCTTTTCT-3′
TNF-α	5′-TCCCAGGTTCTCTTCAAGGGA-3′	5′-GGTGAGGAGCACGTAGTCGG-3′
CCL2	5′-GCAGCAGGTGTCCCAAAGAA-3′	5′-GGTCAGCACAGACCTCTCTCTTG-3′
CXCL10	5′-GGCCATAGGGAAGCTTGAAAT-3′	5′-TCGTGGCAATGATCTCAACAC-3′
Occludin	5′-TGTGGGATAAGGAACACATTTATGA-3′	5′-CAGACACATTTTTAACCCACTCTTCA-3′
Claudin-5	5′-TCTGCTGGTTCGCCAACAT-3′	5′-CGGCACCGTCGGATCA-3′
ZO-1	5′-TGAACGCTCTCATAAGCTTCGTAA-3′	5′-ACCGTACCAACCATCATTCATTG-3′
VE-cadherin	5′-GCGCAGCATCGGGTACTC-3′	5′-GCTTGGTTATTCGGAAGAATTGG-3′
MHV N	5′-TGGAAGGTCTGCACCTGCTA-3′	5′-TTTGGCCCACGGGATTG-3′

follows: (microgram of NaF in the brain/milligram of brain)/(microgram of NaF in sera/microliter of blood). Data are expressed as fold increase in fluorescence compared to the levels in uninfected mice.

siRNA transfections. bEnd.3 cells were seeded in collagen-treated 24-well plates at 60,000 cells/ml and transfected with 25 nM small interfering RNA (siRNA) Flexitube premix (Qiagen, Cambridge, MA) targeting Toll-like receptor 2 (TLR2) mRNA (target sequence, CTCGTTCTCCAGCATTTAAA), CEACAM1a mRNA (target sequence, CACACTCATGCATTCACTCTA), caveolin-1 mRNA (target sequence, ATGGTTTGTCTTGATCAAGAA), or clathrin mRNA (target sequence, CACGTGTTATGGAGTATATTA) or transfected with the AllStars negative-control siRNA (Qiagen, Cambridge, MA) as a nonsilencing transfection control for 36 h prior to infections.

Transendothelial electrical resistance and *in vitro* permeability assays. bEnd3 cell monolayers were grown on collagen-treated 6.5-mm-diameter Transwell polycarbonate membrane inserts (6×10^4 cells/cm^2) (0.4-μm pore size; Costar, Corning, Tewksbury, MA) assembled into 24-well plates and infected for 24 to 72 h. Transendothelial electrical resistance (TEER) (ohms per square centimeter), reflecting barrier integrity, was recorded using an EVOM volt ohmmeter (World Precision Instruments, Sarasota, FL) and calculated by subtracting the resistance of blank inserts from that of the inserts with cells and multiplying the subtracted values by the area of the insert. Barrier function was further analyzed by measuring the permeability of the cell monolayer to sodium fluorescein (molecular mass of 376 Da) and Evans blue (EVB)-labeled albumin (molecular mass of 67 kDa) (Sigma-Aldrich, St. Louis, MO). Ringer-HEPES was added to the abluminal side, while the luminal side was loaded with Ringer-HEPES containing 200 μg/ml NaF, 170 μg/ml EVB, and 10 mg/ml bovine serum albumin (BSA). The cells were incubated at 37°C for 30 min, and the levels of NaF and EVB in the abluminal side were measured using a fluorometer (Biotek, Winooski, VT) with an excitation/emission wavelength ratio of 485/530 nm for NaF and an excitation/emission wavelength ratio of 540/680 nm for EVB. NaF and EVB concentrations were determined using a standard curve.

Immunochemistry. bEnd.3 cells were seeded in collagen-treated two-well Labtek chamber slides and infected for 48 h. The cells were fixed with 3.7% paraformaldehyde (PFA) for 10 min at room temperature, permeabilized with 0.3% Triton X-100, and blocked with 3% BSA. The cells were incubated with primary antibodies (ZO-1, occludin, and VE-cadherin antibodies diluted 1:100; all antibodies from LSBio, Seattle, WA) overnight at 4°C, then incubated with fluorescein isothiocyanate (FITC)-labeled goat anti-rabbit secondary antibody (1:500) (1 h at room temperature), and mounted in antifade medium containing 4′,6′-diamidino-2-phenylindole (DAPI) counterstain (Invitrogen, Ontario, Canada). Fixed cells were imaged with a Zeiss LSM700 static Observer Z1 confocal microscope (63×) (Zeiss, Toronto, Ontario, Canada) and analyzed using ZEN 2009 software. For brain immunolocalization of ZO-1, VE-cadherin, and occludin, mouse brain sections (5 μm) were fixed in paraformaldehyde and embedded in paraffin and the antigens were retrieved by incubating the sections with primary antibodies (1, 2.5, and 10 μg/ml, respectively; all antibodies from LSBio, Seattle, WA) for 1 h in a Ventana automated machine (Ventana Medical Systems, Tucson, AZ), and OmniMap anti-rabbit secondary antibodies conjugated to horseradish peroxidase (HRP) (RUO) for 16 min. The sections were then counterstained with hematoxylin.

Statistical analyses. Data are expressed as means ± standard errors of means. *In vitro* statistical analyses were performed with Student's *t* test comparing the values for mock-infected cells to the values for MHV-infected cells; for experiments with siRNAs, the values for treated MHV-infected cells were compared to the values for untreated MHV-infected cells. *In vivo* statistical analyses were conducted with a one-way analysis of variance (ANOVA) test followed by a *posthoc* Tukey analysis using software program PASW version 18 (IBM SPSS Inc., Chicago, IL). MHV-infected mice were compared to mock-infected mice or MHV3-infected mice were compared to MHV-A59- and 51.6-MHV3-infected mice according to experiments. *P* values of ≤0.05 were considered significant.

RESULTS

Brain invasion by hematogenously spread MHVs correlates with strain virulence and tropism for liver. The discrepancies regarding brain invasion by the highly hepatotropic MHV3 or the weakly hepatotropic MHV-A59 following hematogenous spread of viruses (i.p. inoculation) suggest strain-specific abilities to traffic across the BBB (15, 16, 22, 25, 29). To verify this hypothesis, C57BL/6 mice were i.p. infected for 72 h with MHV3, its attenuated 51.6-MHV3 variant or MHV-A59, and the brains were harvested, stained for histopathological analyses, and assayed for viral detection. Examination of hematoxylin-eosin (HE)-stained brain sections revealed the low-level presence of inflammatory cells in the meninges, microvasculature, and ependymal tissue lining the ventricles in the brains of MHV3-infected mice (Fig. 1A). No inflammatory cells or abnormalities in the neural tissue and choroid plexus were detected in the brains of 51.6-MHV3- or MHV-A59-infected mice. In addition, no multinucleate or rounding cells usually observed in the livers of MHV-infected mice were noted in the brains of all infected mice. Histopathological analysis of the liver was also done from 24 to 72 h p.i. to confirm that viral infection first occurred in the liver following i.p. inoculation in all groups of mice. Multiple foci of inflammatory infiltrations and hepatocyte necrosis were noted as soon as 24 h p.i. and extended until 72 h p.i. in the livers of MHV3-infected mice, while only a few localized foci of necrotic cells were present in the livers of MHV-A59- or 51.6-MHV3-infected mice (results not shown).

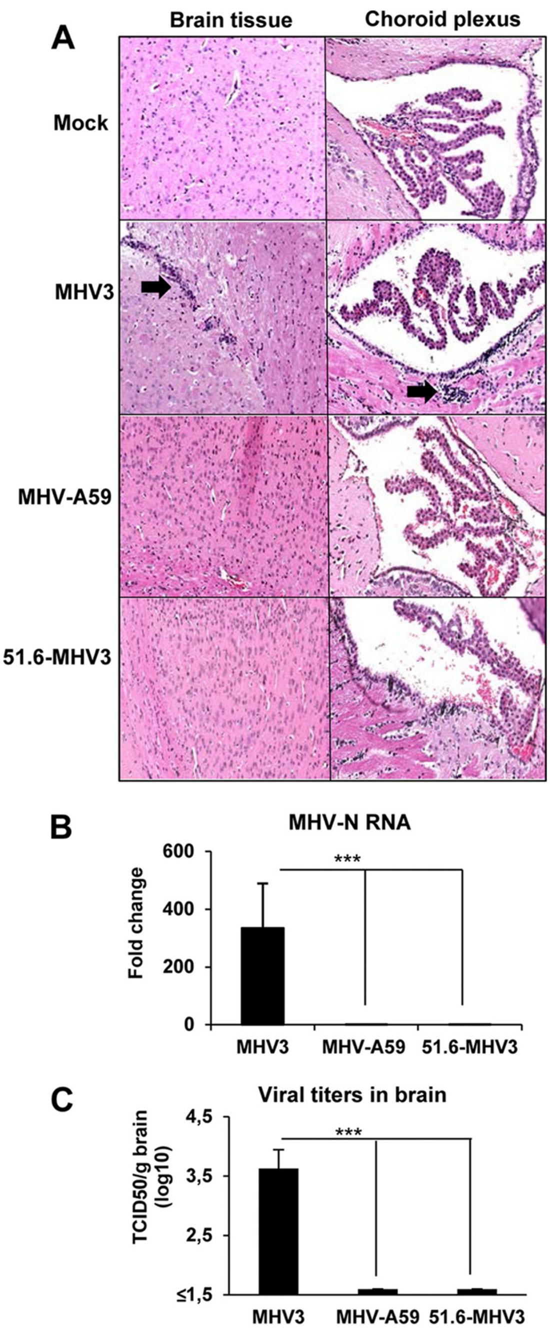

FIG 1 Brain invasion by hematogenously spread MHVs correlates with virulence. (A) Groups of six or seven mice were i.p. mock infected (PBS) or infected with 1,000 $TCID_{50}$ (50% tissue culture infective doses) of MHV3, MHV-A59, and 51.6-MHV3 for 72 h, and harvested brains were subjected to hematoxylin-eosin-safranin staining for histopathological analyses. (B) Viral detection of MHV3, MHV-A59, and 51.6-MHV3 at 72 h p.i. in brain samples of infected mice determined by qRT-PCR analysis of the viral nucleoprotein (N) expression and viral titration ($TCID_{50}$). The viral detection threshold is 1.6 $TCID_{50}$/ml. Values are means plus standard errors of means (error bars). Values that are significantly different ($P < 0.001$) are indicated (***).

Trafficking of virus to the brain was assessed by detection of MHV nucleoprotein (N) RNAs and titration of infectious particles. Viral RNAs and virus titers were detected only in the brains of highly hepatotropic MHV3-infected mice, while no evidence of replication of MHV-A59 and 51.6-MHV3 was noted (Fig. 1B and C). Viral replication level in the brain after 72 h p.i., was, however, too low to permit significant immunolabeling of virally infected cells. Similarly, infectious viruses were titrated at 72 h p.i. in the livers of all groups of mice and demonstrated that MHV3 replicated higher (6.3 ± 0.1 $\log_{10}$ $TCID_{50}$/g liver) than MHV-A59 (3.9 ± 0.16 $\log_{10}$ $TCID_{50}$/g liver) and 51.6-MHV3 (3.6 ± 0.17 $\log_{10}$ $TCID_{50}$/g liver). These results suggest that only the highly hepatotropic MHV3 may have the ability to invade the brain by hematogenous spread and to cross the BBB.

Breakdown of the BBB and alteration of tight junctions occur only in the brains of highly hepatotropic MHV3-infected mice. To further investigate whether MHV3 but not 51.6-MHV3 or MHV-A59 viral replication in the brain following liver infection was due to a breakdown of the BBB, assessment of BBB permeability was performed in mice infected for 72 h with each virus and injected i.p. with 10% NaF dye 1 h prior to euthanasia. The leakage of NaF from the peripheral circulation into the brain is allowed only when the BBB is compromised (30). As shown in Fig. 2A, NaF levels increased in the brains of MHV3-infected mice, indicating a breakdown of the BBB ($P \leq 0.05$). No significant difference in NaF uptake was observed in mice infected with MHV-A59 and 51.6-MHV3.

Since the integrity of the tight junctions is crucial for maintaining the function of the BBB, we asked whether breakdown of the BBB following MHV3 infection resulted from decrease in tight-junction proteins. To assess this, mRNA expression of tight-junction proteins (claudin-5, VE-cadherin, occludin, and ZO-1) was evaluated in the brains of infected mice at 72 h p.i. by qRT-PCR. Compared to brains from mock-infected mice, the level of expression of occludin mRNA was significantly reduced by about 50% in the brains of MHV3-infected mice, but not MHV-A59- or 51.6-MHV3-infected mice ($P \leq 0.01$) (Fig. 2B). The levels of expression of ZO-1 and VE-cadherin mRNA were also impaired in the brains of MHV3-infected mice and to a lesser extent in MHV-A59-infected mice ($P \leq 0.05$ to 0.01), but not in 51.6-MHV3-infected mice (Fig. 2C and D). No significant change in claudin-5 expression was evidenced in mice infected with either virus (Fig. 2E).

To confirm that reduction in tight-junction mRNA expression in the brain was in accordance with a concomitant decrease in protein expression, immunohistochemistry (IHC) stainings using specific antibodies to each protein were conducted on brain tissue. VE-cadherin, occludin, and ZO-1 staining intensities were lower in brain microvessels from MHV3-infected mice than in brain microvessels from mock-infected mice, as shown by the black arrows (Fig. 2F). Lower reduced expression of VE-cadherin and ZO-1 was also detected in the brains of MHV-A59-infected mice, while no change in tight-junction protein expression was induced by 51.6-MHV3 infection.

BMECs (bEnd.3 cell line) are more permissive to MHV3 replication than to 51.6-MHV3 and MHV-A59 replication. Decrease in tight-junction protein expression may result from direct permissivity of BMECs to viral replication and subsequent virus-induced cell damage (31). To determine whether specific MHV3-induced breakdown of the BBB and alteration of tight-junction expression resulted from a differential permissivity of BMECs to MHV infections, *in vitro* infections with MHV3, 51.6-MHV3, and MHV-A59 at an MOI of 0.1 were conducted on a BMEC cell line (bEnd.3 cells) known to exhibit properties similar to those of pri-

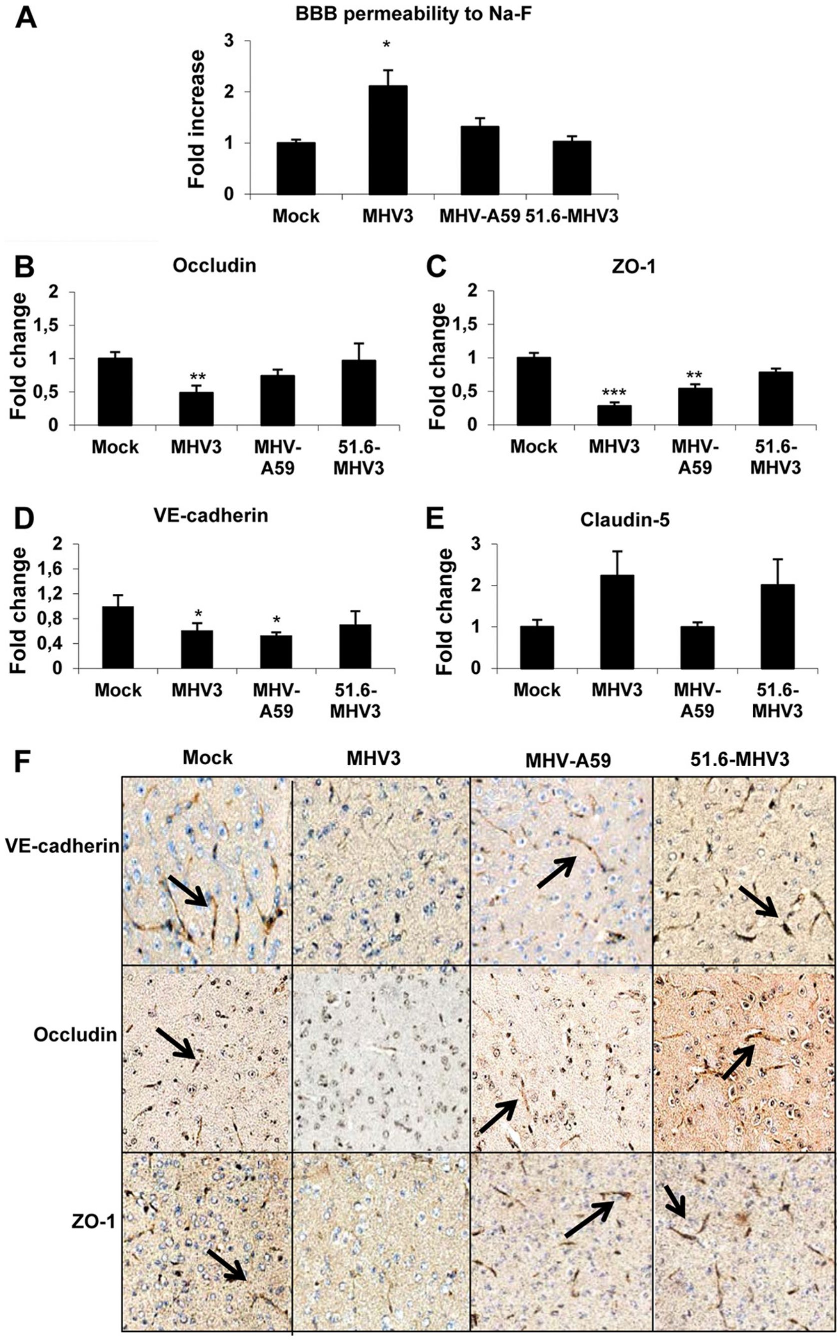

FIG 2 MHV3, but not MHV-A59 and 51.6-MHV3, induces BBB breakdown. Groups of six or seven mice were i.p. mock infected (PBS) or infected with 1,000 $TCID_{50}$ of MHV3, MHV-A59, and 51.6-MHV3 for 72 h. (A) Determination of BBB permeability assessed by sodium fluorescein (NaF) uptake 1 h prior to euthanasia. (B to E) mRNA expression of occludin (B), ZO-1 (C), VE-cadherin (D), and claudin-5 (E) was evaluated in brain samples by qRT-PCR. Values represent fold change in gene expression relative to mock-infected mice after normalization with HPRT expression. All samples were run in duplicate. Values that are significantly different from the value for mock-infected mice are indicated by asterisks as follows: *, $P < 0.05$; **, $P < 0.01$; ***, $P < 0.001$. (F) Immunohistochemistry stainings of VE-cadherin, occludin, and ZO-1 on brain sections of MHV3-, MHV-A59- and 51.6-MHV3-infected mice.

mary BMECs (32, 33). The kinetics of viral replication showed that production of infectious MHV3 increased from day 2 to day 3 p.i. and then stabilized up to day 8 p.i. (Fig. 3A). Viral titers of MHV-A59, unlike MHV3, steadily decreased over time after a rapid increase in the first 3 days ($P \leq 0.01$). As expected, the 51.6-MHV3 variant, expressing low tropism for liver endothelial cells (17), showed a delayed replication in bEnd.3 cells, as evidenced by the absence of infectious virus production until day 3 p.i., followed by a lower viral replication level ($P \leq 0.01$). Occurrence of few foci of cytopathic effects, characterized by rounded cells instead of typical "cobblestone" morphology, were noted in MHV3- and MHV-A59-infected cell cultures, but no typical MHV-induced giant syncytial cells or cell lysis was observed (not shown).

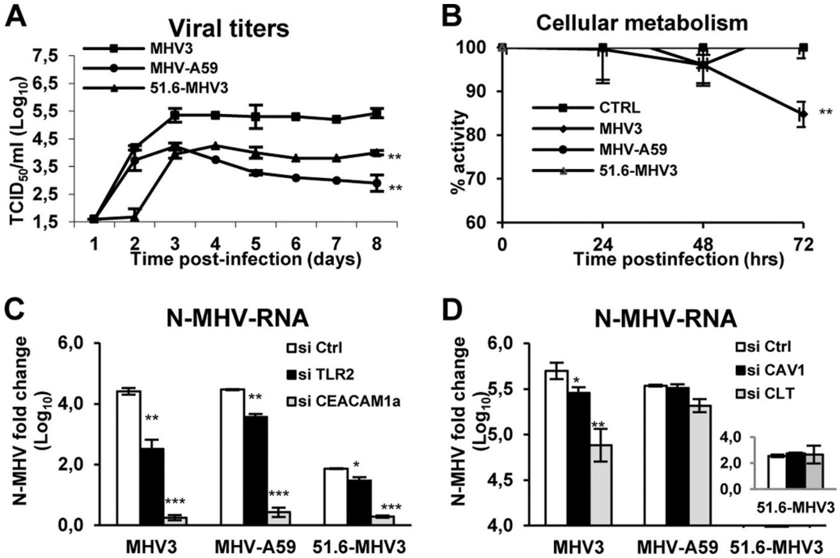

FIG 3 MHV3 exhibits higher tropism for BMECs than MHV-A59 and 51.6-MHV3 do. Mouse bEnd.3 immortalized brain microvascular endothelial cells (BMECs) were infected with MHV3, MHV-A59, or 51.6-MHV3 at an MOI of 0.1. (A) Kinetics of MHV infections up to 8 days p.i. (B) Metabolic activity of infected BMECs as determined by MTS-PMS colorimetric assay from 24 h to 72 h p.i. (C) Roles of CEACAM1a and TLR2 in MHV entry into BMECs. (D) Roles of caveolin-1 (CAV-1) and clathrin (CLT) in MHV endocytosis by BMECs. bEnd.3 cells were treated with specific siRNA to each molecule prior to infection for 24 h, and MHV nucleoprotein (N) mRNA expression was determined by qRT-PCR. All experiments were conducted in triplicate. Results are representative of two or three independent experiments. Values are means ± standard errors of means (error bars). Values that are significantly different are indicated by asterisks as follows: *, $P < 0.05$; **, $P < 0.01$; ***, $P < 0.001$. CTRL and Ctrl, control (uninfected cells).

In order to confirm low or no major changes in cellular metabolism in the first 72 h of infection in MHV3-, MHV-A59-, or 51.6-MHV3-infected BMECs, the metabolic activity of infected bEnd.3 cells was evaluated using the 3-(4,5-dimethylthiazol-2-yl)-5-(3-carboxymethoxyphenyl)-2-(4-sulfophenyl)-2H-tetrazolium inner salt) (MTS)-phenazine methosulfate (PMS) colorimetric assay from 24 h to 72 h p.i. and compared to uninfected control cells. The percentage of optical density (OD), compared with control cells, slowly decreased (about 15%) in the first 72 h p.i. only in MHV3-infected bEnd.3 cells ($P \leq 0.01$) (Fig. 3B). In addition, the loss of cell activity did not increase when cells were infected with a higher MOI (MOIs of 1 and 5) (results not shown).

Higher permissivity of BMECs to MHV3 depends on CEACAM1a and TLR2 ligation and on both clathrin- and caveolin-dependent endocytosis for entry, in contrast to 51.6-MHV3 and MHV-A59. It was previously shown that the protective role of the BBB against brain invasion by blood-borne MHV-A59 was related to a specific blockade of viral entry in BMECs (22). Fixation and entry of MHVs in target cells generally depend on fixation of viral S protein to the common MHV receptor CEACAM1a and further endocytosis or fusion with the host cell (23). However, we have also previously demonstrated that S protein from MHV3 can ligate to TLR2 on the macrophage cell surface (34). To provide insight into how MHV3 exhibits differential viral fixation and/or entry into BMECs compared to MHV-A59 and 51.6-MHV3, the levels of MHV nucleoprotein (N) RNA, as an indicator of viral entry and/or subsequent replication, were evaluated in bEnd.3 cells following abrogation of CEACAM1a or TLR2 expression by specific siRNAs. As shown in Fig. 3C, abrogation of the CEACAM1a expression resulted in a substantial decrease of MHV N RNA expression in BMECs infected with all viruses ($P \leq 0.001$). Knockdown of TLR2 expression, however, provoked a higher decrease of viral replication in MHV3-infected cells ($P \leq 0.01$) than in MHV-A59- and 51.6-MHV3-infected cells ($P \leq 0.01$ and $P \leq 0.05$, respectively), suggesting a more important role for TLR2 in the fixation or entry of MHV3 in BMECs.

It has already been demonstrated that restriction of the BBB to weakly hepatotropic MHV-A59 virus entry was abrogated by SDS detergent treatment (22), suggesting that restriction of MHV-A59 entry in BMECs occurred at the endocytosis step (35). It is thus proposed that MHV3, in contrast to MHV-A59, takes advantage of caveolin- and/or clathrin-dependent endocytic pathways to infect BMECs. To address this, bEnd.3 cells were treated with siRNAs for clathrin or caveolin-1 prior to infection by all MHV strains. As shown in Fig. 3D, MHV N RNA levels decreased in MHV3-infected cells when clathrin or caveolin-1 expression was abrogated ($P \leq 0.05$ to 0.01), while MHV N RNA levels of MHV-A59 were altered only in clathrin-deficient, infected cells ($P \leq 0.05$), suggesting that MHV3, in contrast to MHV-A59, may use both endocytic pathways for viral entry into BMECs. No significant effect was observed in 51.6-MHV3-infected cells, due to no or low viral RNA level.

MHV3, but not MHV-A59 and 51.6-MHV3, enhances *in vitro* permeability of BMECs, leading to viral transendothelial migration. We further investigated whether MHV3 infection might affect *in vitro* the barrier functions of BMECs, such as observed *in vivo* above. To address this, an *in vitro* model of BBB was constructed using bEnd.3 cell monolayers growing on Transwell inserts as previously described (32, 33). First, cells were infected with MHV strains for 24 to 72 h, and transendothelial electrical resistance (TEER), reflecting BBB integrity, was monitored. TEER decreased at 48 and 72 h p.i. in MHV3-infected BMECs ($P \leq 0.05$ to 0.01), while it was weakly affected at 72 h p.i. only in MHV-A59-infected cells ($P \leq 0.05$) (Fig. 4A). The 51.6-MHV3 infection did not alter the TEER.

Thereafter, to determine whether such alteration of TEER in

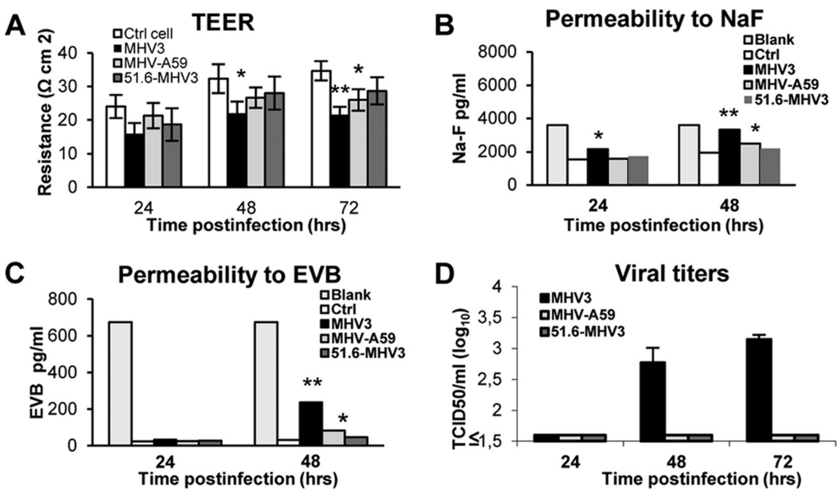

FIG 4 MHV3, but not MHV-A59 and 51.6-MHV3, alters *in vitro* BMEC barrier integrity. An *in vitro* model of BBB was constructed using bEnd.3 cell monolayers grown on Transwell inserts, and cells were infected with MHV3, MHV-A59, or 51.6-MHV3 at an MOI of 0.1. (A) Transendothelial electrical resistance (TEER), reflecting barrier integrity, was monitored from 24 to 72 h. (B and C) Evaluation of the paracellular permeability of bEnd.3 monolayers to NaF (B) or Evans blue (C) dye at 24 and 48 h p.i. Blank corresponds to maximal permeability (insert without cells). (D) Determination of viral transmigration across the bEnd.3 monolayer. Viral titers were recorded in the basolateral chamber from 24 to 72 h p.i. The Viral detection threshold is 1.6 $TCID_{50}$. All experiments were conducted in triplicate. Results are representative of two independent experiments. Values that are significantly different are indicated by asterisks as follows: *, $P < 0.05$; **, $P < 0.01$.

MHV3-infected bEnd3 cells correlated with enhanced paracellular permeability, extravasation of the fluorescent NaF dye through infected bEnd.3 cell monolayers was evaluated in the basolateral chamber. NaF uptake was significantly increased in MHV3-infected monolayers as soon as 24 h p.i. and extended to 48 h p.i., indicating considerable effects on BBB paracellular permeability ($P \leq 0.05$ to 0.01) (Fig. 4B). MHV-A59 infection, however, induced a slight increase of NaF uptake at 48 h p.i. only ($P \leq 0.05$). To further characterize the extent of damage induced by MHV3 infection on BMEC permeability, extravasation of the high-molecular-weight Evans blue (EVB) dye was assessed. Albeit to a lesser extent than NaF, a higher uptake of EVB was found in MHV3-infected bEnd.3 monolayers ($P \leq 0.01$) than in MHV-A59-infected bEnd.3 monolayers ($P \leq 0.05$) (Fig. 4C). No effect on the permeability to either dye was noted in 51.6-MHV3-infected cells. Finally, we postulated that MHV3-induced enhancement of permeability would allow the virus to transmigrate across the bEnd.3 monolayer, so we assessed infectious virus titers in the basolateral chamber. As shown in Fig. 4D, MHV3 viral titers (more than 1.6 $\log_{10}$ units), but not MHV-A59 or 51.6-MHV3 viral titers, were detected at 48 and 72 h p.i. in the basolateral chamber, indicating that only MHV3 exhibited the ability to cross the *in vitro* BMEC barrier.

Breakdown of the *in vitro* BMEC barrier by MHV3 results from decreased expression of occludin, VE-cadherin, and ZO-1 tight-junction proteins. To further determine whether MHV3-induced impairment of barrier function of BMECs was associated with alteration of tight junctions in BMECs, such as observed above in the brains of infected mice, the levels of expression of claudin-5, ZO-1, VE-cadherin, and occludin mRNA were evaluated in infected bEnd.3 cells by qRT-PCR at 48 h p.i. Significant reduction of occludin, VE-cadherin, and ZO-1 mRNA expression occurred in MHV3-infected BMECs only ($P \leq 0.05$) (Fig. 5A, B, and C). Claudin-5 mRNA expression in BMECs, however, was not affected by MHV3 or other virus strains (Fig. 5D).

To confirm that such reduction in mRNA expression of tight junctions was consistent with a reduction in protein expression, immunofluorescence staining was performed on infected cells. In comparison to uninfected cells (control), the intensity of surface staining of VE-cadherin and ZO-1 as well as cytoplasmic and nuclear staining of occludin decreased in MHV3-infected BMECs, while no apparent difference was noted in either MHV-A59- or 51.6-MHV3-infected cells (Fig. 5E).

MHV3-induced breakdown of the *in vitro* BMEC barrier does not depend on inflammatory factors. BBB disruption during viral infection may be indirectly provoked by virus-induced inflammatory mediators, such as the cytokines TNF-α and IL-6 or chemokines CCL2 and CXCL10 (1, 5–8). Accordingly, we hypothesized that MHV3 infection, but not MHV-A59 and 51.6-MHV3 infections, may increase the production of autocrine inflammatory factors by BMECs that might subsequently compromise BBB integrity. To address this, the levels of TNF-α, IL-6, CCL2, and CXCL10 were evaluated in MHV-infected bEnd.3 cells by qRT-PCR and ELISAs at 24 h p.i. As shown in Fig. 6A and B, mRNA levels of TNF-α did not increase in MHV3-infected cells, in contrast to 51.6-MHV3- and MHV-A59-infected cells ($P \leq 0.05$), although protein expression was not detected by ELISA. Transcription and production of IL-6, however, increased in 51.6-MHV3- and MHV-A59-infected cells ($P \leq 0.05$ to 0.001) (Fig. 6C and D), but not MHV3-infected cells. The production of CCL2 increased only in 51.6-MHV3-infected cells ($P \leq 0.01$ to 0.001) (Fig. 6E and F), while CXCL10 levels were not induced in any MHV-infected cells (Fig. 6G and H). Taken together, these results suggest that barrier breakdown by MHV3 infection does not correlate with induction of inflammatory factors, which are instead produced by 51.6-MHV3- and MHV-A59-infected cells.

MHV3-induced breakdown of *in vitro* BMEC barrier is related to impaired production of IFN-β by infected cells. It was demonstrated that IFN-β promotes BBB integrity and prevents virus-induced barrier breakdown (36, 37). Accordingly, we hy-

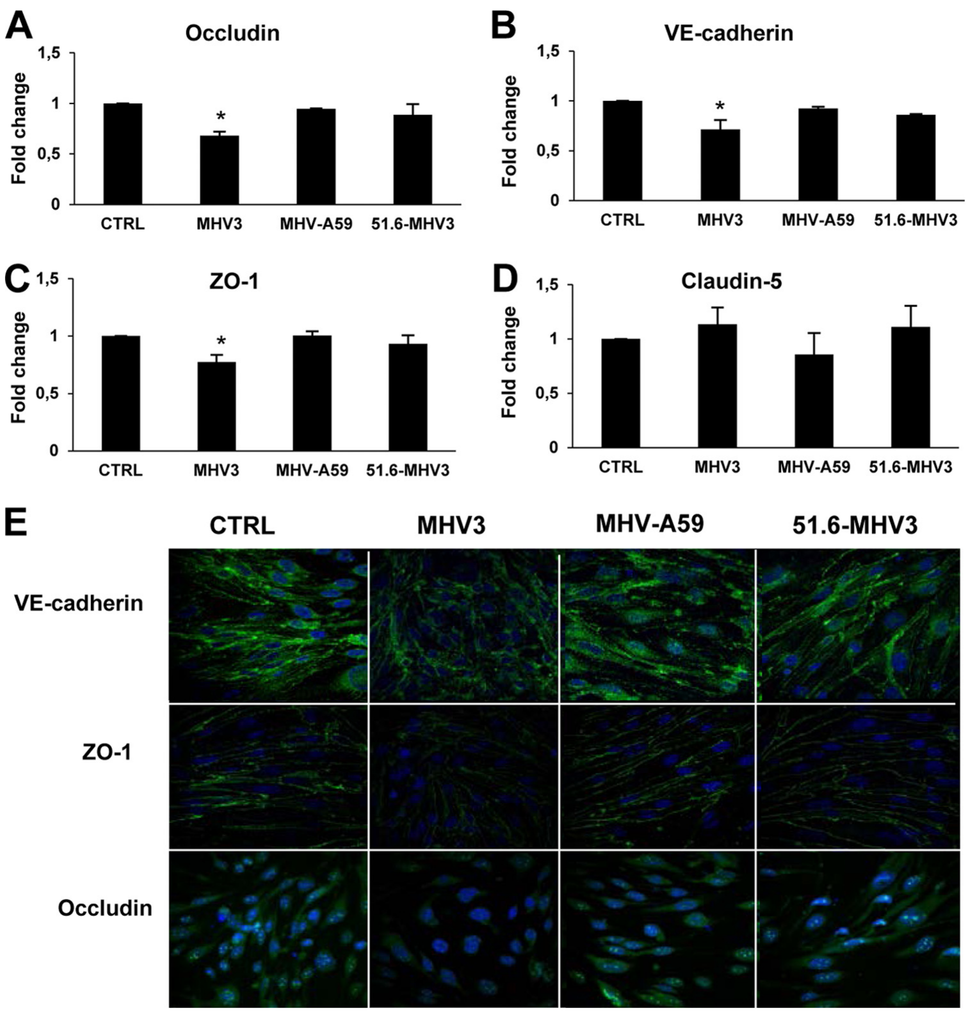

FIG 5 MHV3, but not MHV-A59 and 51.6-MHV3, alters tight-junction expression on BMECs. (A to D) bEnd.3 cells were infected for 48 h with MHV3, MHV-A59, and 51.6-MHV3 at an MOI of 0.1, and the levels of expression of occludin (A), VE-cadherin (B), ZO-1 (C), and claudin-5 (D) mRNA were evaluated by qRT-PCR. Values represent fold change in gene expression relative to uninfected cells (control [CTRL]) after normalization with HPRT expression. All samples were run in duplicate. All experiments were conducted in triplicate. Results are representative of two independent experiments. Values that are significantly different ($P < 0.05$) are indicated (*). (E) Immunofluorescence stainings of the tight-junction (green) VE-cadherin, occludin, and ZO-1 and the nucleus (blue) in uninfected (CTRL) and infected bEnd.3 cells. Images presented are from one representative experiment out of three independent experiments.

pothesized that MHV-A59 or 51.6-MHV3, but not MHV3, induced barrier protective IFN-β production by BMECs. As expected, higher levels of mRNA and secreted IFN-β were detected in 51.6-MHV3- and MHV-A59-infected cells ($P \leq 0.05$ to 0.001) than in MHV3-infected cells ($P \leq 0.05$) (Fig. 7A and B).

To confirm that barrier disruption during MHV3 infection results from the absence of IFN-β production, we evaluated the barrier properties of bEnd.3 cell monolayers upon MHV infections in the presence of IFN-β (100 pg/ml) or anti-IFN-β antibodies (1 μg/ml) at 48 h p.i. As observed in Fig. 7C, addition of IFN-β increased the TEER both in control (uninfected) and MHV-infected cultures, which is in concordance with its barrier enhancing properties ($P \leq 0.05$ to 0.01). TEER decreased only in MHV3-infected cells but was completely restored by IFN-β treatment ($P \leq 0.01$) (Fig. 7C). However, addition of anti-IFN-β antibodies did not decrease TEER in spite of a nonsignificant decrease in 51.6-MHV3-infected cells. Moreover, previously observed enhancement of paracellular permeability to NaF and EVB in MHV3-infected cells and to a lesser extent in MHV-A59-infected cells at 72 h p.i. was abolished following the addition of IFN-β ($P \leq 0.01$ and $P \leq 0.05$, respectively) (Fig. 7D and E), while anti-IFN-β treatment increased paracellular permeability in weakly hepatotropic MHV-A59- and 51.6-MHV3-infected BMECs compared with untreated infected cells ($P \leq 0.01$ and $P \leq 0.05$, respectively).

In order to confirm that the rescued barrier properties of infected bEnd.3 cells following IFN-β treatment result from preservation of tight-junction protein expression, the levels of expression of occludin, ZO-1, and VE-cadherin mRNA were analyzed by qRT-PCR. As shown in Fig. 7F to H, the addition of IFN-β to MHV3-infected cells abolished the decreases in expression of occludin, ZO-1, and VE-cadherin genes ($P \leq 0.05$ to 0.01) and blocked MHV3 trafficking across the bEnd.3 monolayer, as no infectious viruses were detected in the basolateral chamber (not shown).

On the other hand, neutralization of IFN-β potentially pro-

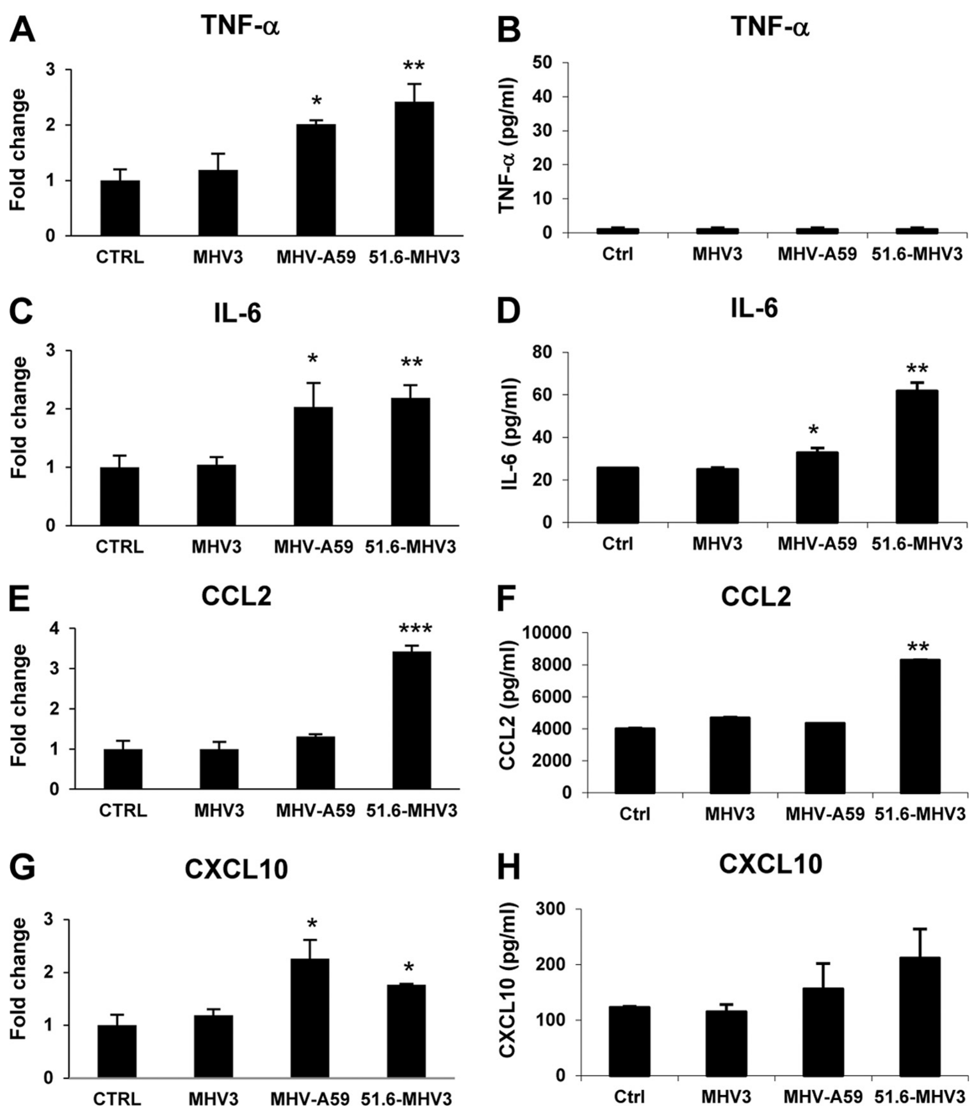

FIG 6 MHV3-induced breakdown of BMEC barrier does not depend on inflammatory factors. (A to H) bEnd.3 cells were infected with MHV3, MHV-A59, and 51.6-MHV3 at an MOI of 0.1, and mRNA expression (A, C, E, and G) and protein levels (B, D, F, and H) of TNF-α, IL-6, CCL2, and CXCL10 were evaluated by qRT-PCR and ELISAs, respectively, at 24 h p.i. All samples were run in duplicate. All experiments were conducted in triplicate. Results are representative of two independent experiments. Values that are significantly different are indicated by asterisks as follows: *, $P < 0.05$; **, $P < 0.01$; ***, $P < 0.001$.

duced in MHV3-infected culture did not worsen virus-induced barrier permeability or reduction of tight junctions (Fig. 7D to H), which is in accordance with the low levels of IFN-β produced by MHV3-infected cells. However, as shown in MHV-A59- and 51.6-MHV3-infected cultures, neutralization of IFN-β increased barrier permeability to NaF and EVB ($P \leq 0.05$ to 0.01), correlating with concomitant reduction of TEER ($P \leq 0.05$) (Fig. 7C to E) and decreased expression of occludin and VE-cadherin in 51.6-MHV3-infected cells, but not in MHV-A59-infected cells ($P \leq 0.05$) (Fig. 7F to H).

To verify whether such improvement of barrier integrity by IFN-β might indirectly result from its antiviral rather than its barrier protective properties, virus titers were assessed in both IFN-β-treated and untreated MHV-infected cells. Viral replication of MHV3 was not blocked by IFN-β treatment, since viral titers remained similar in untreated and IFN-β-treated infected cells (4.6 ± 0.3 and 4.3 ± 0.3 $\log_{10}$ $TCID_{50}$/ml, respectively), while MHV-A59 replication was completely abolished in IFN-β-treated cells (from 3.9 ± 0.33 to <1.6 $\log_{10}$ $TCID_{50}$/ml). Moreover, neutralization of IFN-β increased viral titers in MHV-A59- and 51.6-MHV3-infected cells (from 3.9 ± 0.33 to 5 ± 0.04 $\log_{10}$ $TCID_{50}$/ml and from <1.6 to 4 ± 0.1 $\log_{10}$ $TCID_{50}$/ml, respectively). In addition, neutralization of IFN-β allowed transit of MHV-A59, but not 51.6-MHV3, across the cell monolayer as evidenced by titers in the basolateral chamber (3.175 ± 0.25 $\log_{10}$ $TCID_{50}$/ml). These results suggest that the amount of IFN-β produced by BMECs upon infection with MHV-A59 and 51.6-MHV3, but not MHV3, may both control viral replication in these cells and prevent induction of BBB breakdown.

DISCUSSION

In this work, we report for the first time that BBB integrity can be impaired during acute liver infection by highly hepatotropic MHV3, but not by weakly hepatotropic MHV-59 and attenuated

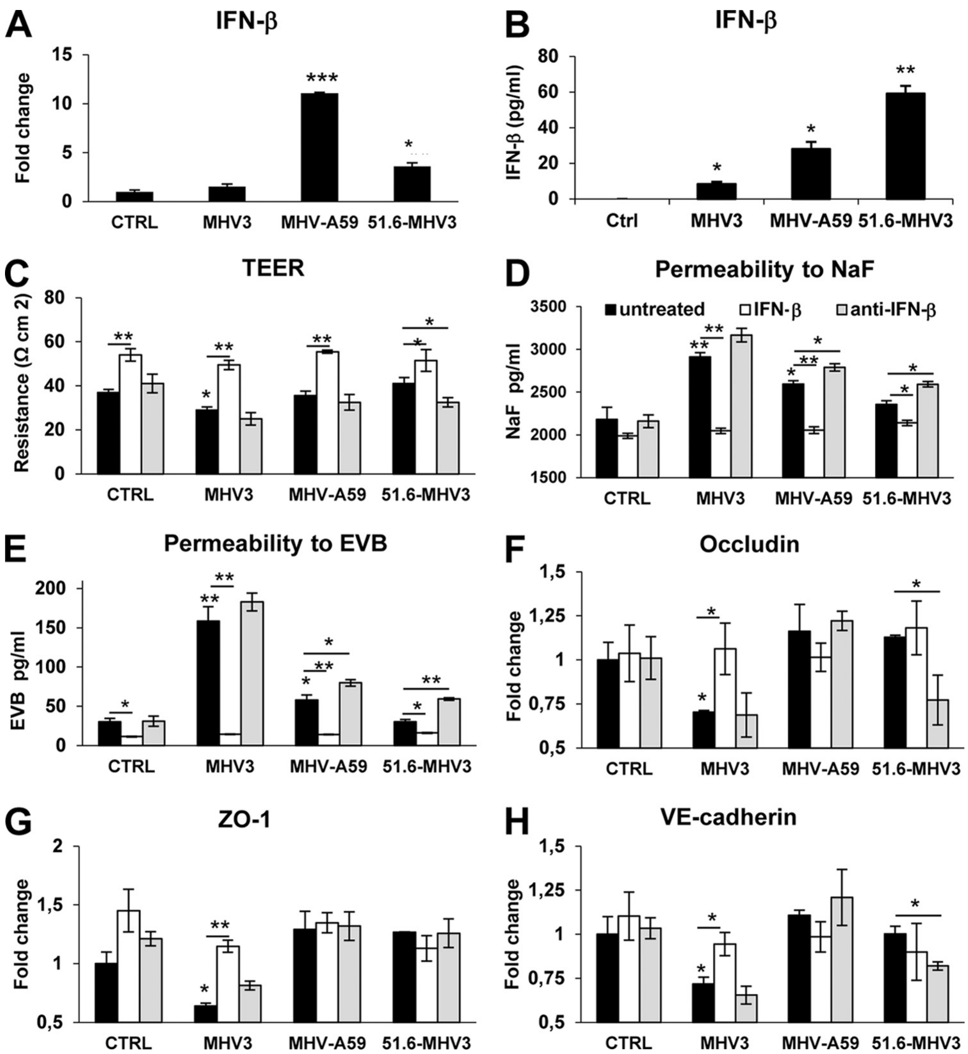

FIG 7 MHV3-induced breakdown of BMEC barrier is related to downregulation of barrier protective IFN-β production by infected BMECs. (A and B) bEnd.3 cells were infected with MHV3, MHV-A59, and 51.6-MHV3 at an MOI of 0.1, and mRNA expression (A) and protein expression (B) of IFN-β was evaluated at 24 h p.i. by qRT-PCR and ELISAs, respectively. All samples were run in duplicate. All experiments were conducted in triplicate. (C to H) Evaluation of barrier integrity of bEnd.3 monolayers infected for 48 h with MHV3, MHV-A59, and 51.6-MHV3 at an MOI of 0.1 in the presence of recombinant IFN-β (100 pg/ml) or anti-IFN-β monoclonal antibodies (1 μg/ml). (C) Recordings of TEER in infected bEnd.3 cultures. (D and E) Evaluation of the paracellular permeability of infected bEnd.3 monolayers to NaF (D) or Evans blue (E) dyes. (F to H) mRNA expression levels of occludin (F), ZO-1 (G), and VE-cadherin (H) in bEnd.3 cells evaluated by qRT-PCR. Values represent fold change in gene expression relative to uninfected cells (control [CTRL]) after normalization with HPRT expression. Results are representative of two independent experiments. Values that are significantly different are indicated by asterisks as follows: *, $P < 0.05$; **, $P < 0.01$; ***, $P < 0.001$.

51.6-MHV3 strains, enabling MHV3 invasion of the CNS. We demonstrated here that MHV strain-specific ability to cross the BBB during acute liver infection correlated with enhanced BBB permeability as evidenced *in vivo* and *in vitro*. Enhanced BBB permeability in MHV3 infection only is associated with higher viral tropism for BMECs and disruption of ZO-1, VE-cadherin, and occludin tight junctions. Such impairment of tight-junction expression was independent of virus-induced barrier-dysregulating TNF-α, IL-6, CCL2, and CXCL10 but rather related to inhibition of barrier protective IFN-β production by BMECs.

Some human respiratory strains of CoVs have shown neuroinvasive properties and were proposed as potential etiological agents for multiple sclerosis (10–12), but their mechanism of neuroinvasion is unclear. The major aim of our work was to investigate the ability of CoVs to enter the CNS through the BBB during the acute phase of infection in peripheral organs. We provide evidence that brain invasion by blood-borne MHVs correlate with strain virulence and peripheral replication in the liver. As previous studies reported the inability of the weakly hepatotropic MHV-A59 strain to induce neurological disease following i.p. infection in contrast to the highly hepatotropic MHV3 (16, 22), we presumed a strain-specific restriction of CNS invasion at the BBB level according to virulence. In agreement, brain examination of i.p. acutely infected mice revealed that viral replication occurred only in the brains of MHV3-infected mice, indicating a specific ability of this strain to enter the CNS by the hematogenous route. Moreover, no replication in the brain of the 51.6-MHV3 variant, having no tropism for endothelial cells (17), suggested that permissivity of cerebral endothelial cells to MHV3 infection played a major role in brain invasion. This strain-specific ability of MHV3 to cross the BBB *in vivo* has been confirmed *in vitro* on a modeled BBB of a bEnd.3 cell monolayer grown on a Transwell system. As expected, only MHV3 transmigrated across the bEnd-3 cell monolayer and reached the basolateral chamber. BBB invasion by MHV3 during acute infection results from enhanced barrier permeability, as evidenced by a higher decrease of TEER and leakage of both the low-molecular-weight NaF and the high-molecular-weight Evans blue dyes in the brains of infected mice and/or BMECs. We would reasonably assume that virus-induced BBB impairment preceded viral brain invasion *in vivo*, since no virus titers were found until 72 h p.i. in the brains, while infectious viruses were detected as soon as 24 h p.i. in the livers of MHV3-infected mice (results not shown). Taken together, these results demonstrate the strain-specific ability of the highly hepatotropic MHV3 to cross the BBB, but not the attenuated 51.6-MHV3 or weakly hepatotropic MHV-A59.

BBB disruption by blood-borne viruses after primary replication in peripheral organs is a common feature of several acute viral infections, but the mechanisms involved have not yet been completely elucidated. Several of these acute viral infections, including murine adenovirus type 1 (MAV-1), human immunodeficiency virus type 1 (HIV-1), West Nile virus (WNV), and lymphocytic choriomeningitis mouse virus (LCMV) infections were reported to trigger increases in BBB permeability through disruption of tight junctions (1, 31, 36). We showed here for the first time that a coronavirus, MHV3, can increase BBB permeability in impairing tight-junction ZO-1, VE-cadherin, and occludin expression in BMECs and the brain. The MHV-A59 or 51.6-MHV3 strain, however, induced no or a slight reduction of ZO-1 and VE-cadherin expression that may reflect their weak tropism for BMECs. No decrease of claudin-5 expression was observed, suggesting that either claudin was not specifically altered by viral infection or that a small decrease in claudin-5 might be masked by the higher number of other claudin family members (38).

Viral replication and/or viral products are rarely directly implicated in BBB disruption (1), but MAV-1 infection itself and the gp120 from HIV were shown to disrupt tight junctions on BMECs (31, 39). Replication of MHV3 in BMECs did not reach high titers and was associated with low cell damage and loss of activity. As expected, ligation to CEACAM1a viral receptor was essential for infection of BMECs by all MHVs, but MHV3 exhibited an additional ability to take advantage of both caveolin- and clathrin-dependent endocytic pathways for entry into BMECs. MHV-A59 entry via clathrin-dependent endocytosis, but not caveolin-dependent endocytosis, has also been previously reported in other cell types (40, 41). TLR2 is located in enriched caveolin-1-associated lipid raft microdomains at the cell surface (42). We have shown that TLR2 engagement by MHV3 on BMECs favored viral replication, which is in agreement with our previous findings that viral S protein of MHV3 can ligate to both CEACAM1a and TLR2 on macrophages (34), in contrast to MHV-A59 (43). Interestingly, as TLR2 activation was shown to increase permeability and downregulate tight-junction protein expression on BMECs (44), TLR2 ligation by viruses or soluble viral coat proteins may represent a new mechanism of BBB disruption by viruses.

Viral fixation and endocytosis pathways also trigger activation of inflammatory cytokines, chemokines, and type 1 interferon according to TLR and/or helicase-dependent downstream signaling pathways (5, 34, 36). Loss of tight junctions in several viral infections can indirectly result from virus-induced barrier-dysregulating cytokines or chemokines, such as IL-6, TNF-α, CCL2, or CXCL10 by BMECs themselves or other CNS cell types (1, 5–8). It was previously shown that MHV3 fixation to TLR2 in macrophages increased TNF-α and IL-6 production (34), but herein, no induction of cytokine and chemokine production by MHV3-infected BMECs was observed. However, cytokine and chemokine production was noted instead in BMECs infected with 51.6-MHV3 and MHV-A59, indicating that BBB breakdown cannot result from virus-induced host inflammatory factors, since BBB was not significantly altered by these two strains. Nevertheless, we cannot rule out the possibility that cytokines and chemokines may be produced *in vivo* by recruited inflammatory cells in the CNS during MHV3 infection and thus contribute to BBB disruption. However, only a few inflammatory cells have been evidenced by hematoxylin-eosin-safranin (HES) staining at 72 h p.i. in the brains of MHV3-infected mice, and the levels of IL-6, TNF-α, CCL2, and CXCL10 were lower in the brains of MHV3-infected mice than in the brains of MHV-A59- and 51.6-MHV3-infected mice (results not shown), thus minimizing the role of inflammatory factors in BBB breakdown.

Postinfection BBB breakdown has already been observed following intracerebral infection of mice with the strictly neurotropic MHV-JHM strain and has been primarily associated with matrix metalloproteinase 9 (MMP-9) produced by infiltrating neutrophils (45). However, in this study, *in vivo* enhancement of BBB permeability was observed only by day 4 p.i. Such discrepancies with our data may result from differences in the route of inoculation and the MHV strain used. It is possible that intracerebral inoculation, which bypasses BBB transit, may have not been conducive to infection of the endothelium by the virus. Herein, we report that MHV3 infection of BMECs can directly alter BBB integrity without assistance of neutrophils and MMPs. We cannot, however, rule out the possibility that later recruited neutrophils may further affect BBB integrity by MMP production once it has been first compromised by viral infection of BMECs. Preliminary data, however, revealed that expression of MMP1a and MMP3 by BMECs was not affected by *in vitro* infection with MHV3, 51.6-MHV3, or MHV-A59 strain.

Unlike inflammatory mediators, IFN-β is known to promote tight-junction formation and stability (37). The differential IFN-β production by BMECs upon infection by MHVs may possibly represent one key factor in MHV strain specificity to induce BBB breakdown. We have shown that 51.6-MHV3 and, to a lesser extent MHV-A59, compared to MHV3, elicited IFN-β production by BMECs, supporting the hypothesis that IFN-β could act as a protective factor in preventing barrier damage and brain invasion by these strains. The lower IFN-β production by cells infected with MHV-A59 may reflect posttranscriptional inhibitory mechanisms of IFN-β production by viral factors (reviewed in reference 46). Induction of IFN-β by WNV has already been reported to prevent its trafficking across a BBB model *in vitro* (36). The specific mechanism of barrier protection by IFN-β is unknown, but Daniels et al. (36) recently reported that IFN-β was able to rescue barrier dysfunction elicited by inflammatory cytokines. Thus, one could speculate that IFN-β production by MHV-A59- and 51.6-MHV3-infected BMECs may counteract cytokine-mediated barrier damage or that low levels of inflammatory cytokines produced by infected BMECs may not be sufficient to induce BBB breakdown. In accordance, activation of type I IFNs by dengue virus was reported to ameliorate inflammatory cytokine-driven barrier dysfunction in peripheral endothelium (47). The importance of IFN-β downregulation in MHV3-induced BBB breakdown is supported by our results showing that the addition of IFN-β antagonized MHV3-mediated permeability and disruption of tight junctions in BMECs independently of its antiviral properties, as viral replication was not altered. Resistance of MHV3 to antiviral properties of type I IFN *in vitro* has already been observed (48). On the other hand, barrier integrity in MHV-A59- and 51.6-MHV3-infected BMEC monolayers was lost when IFN-β was neutralized with monoclonal antibodies, confirming that prevention of BBB breakdown during MHV-A59 and 51.6-MHV3 infection is due at least partly to IFN-β production. Moreover, in contrast to MHV3, replication of MHV-A59 and 51.6-MHV3 was lowered by IFN-β, suggesting that BMECs can control replication of these viral strains through IFN-β production. This is in agreement with previous findings showing no appearance of productive replication of MHV-A59 in BMECs *in vivo* (22, 25).

Hence, the results of this study show for the first time that hematogenously spread mouse coronaviruses can invade the CNS at the BBB level following peripheral primary replication. Earlier and higher replication of MHV3 in the liver (not shown), combined with higher permissivity of BMECs to MHV3 infection, may potentiate BBB breakdown and further brain invasion. On the other hand, preservation of BBB integrity in MHV-A59 and 51.6-MHV3 infection prevents their trafficking from the periphery to the CNS. This hypothesis is supported by a previous report showing that MHV-A59 spread to the brain is allowed only after intravenous (i.v.) injection of sodium dodecyl sulfate detergent into the mice, which is presumed to alter BBB integrity (22).

In human infections, the mechanism involved in CNS invasion by CoVs following primary infection in the upper respiratory tract is unclear. The CoV 229E strain was previously reported to infect BMECs (49), suggesting that BBB invasion by human CoVs is probable.

The mechanism(s) used by MHV3 to block the production of IFN-β by BMECs is not yet known. The absence of cytokine and chemokine production by MHV3-infected BMECs, in contrast to MHV-A59- and 51.6-MHV3-infected BMECs, suggests that MHV3 may specifically evade detection by TLRs or helicases and/or signaling downstream pathways in BMECs. Accordingly, Mazaleuskaya et al. (50) have recently shown that stimulation of TLR-2, TLR-4, and TLR-7 by specific agonists had no effect on MHV3 replication. Further research is needed to confirm viral evasion mechanisms used by MHV3 in BMECs and their effects on BBB disruption.

ACKNOWLEDGMENTS

We thank Dominic Fillion and Pascale Bellaud for technical assistance with confocal microscopy and histochemistry, respectively, and Antony Karelis for revision of the manuscript.

This work was funded by grants from NSERC, which is funded by the Government of Canada. Christian Bleau was supported by an NSERC fellowship.

REFERENCES

1. **Spindler KR, Hsu TH.** 2012. Viral disruption of the blood-brain barrier. Trends Microbiol **20:**282–290. http://dx.doi.org/10.1016/j.tim.2012.03.009.
2. **Hase T, Dubois DR, Summers PL.** 1990. Comparative study of mouse brains infected with Japanese encephalitis virus by intracerebral or intraperitoneal inoculation. Int J Exp Pathol **71:**857–869.
3. **Kobiler D, Lustig S, Gozes Y, Ben-Nathan D, Akov Y.** 1989. Sodium dodecylsulphate induces a breach in the blood-brain-barrier and enables a West Nile virus variant to penetrate into mouse brain. Brain Res **496:**314–316. http://dx.doi.org/10.1016/0006-8993(89)91079-2.
4. **Lustig S, Danenberg HD, Kafri Y, Kobiler D, Ben-Nathan D.** 1992. Viral neuroinvasion and encephalitis induced by lipopolysaccharide and its mediators. J Exp Med **176:**707–712. http://dx.doi.org/10.1084/jem.176.3.707.
5. **Wang T, Town T, Alexopoulou L, Anderson JF, Fikrig E, Flavell RA.** 2004. Toll-like receptor 3 mediates West Nile virus entry into the brain causing lethal encephalitis. Nat Med **10:**1366–1373. http://dx.doi.org/10.1038/nm1140.
6. **Afonso PV, Ozden S, Prevost MC, Schmitt C, Seilhean D, Weksler B, Couraud PO, Gessain A, Romero IA, Ceccaldi PE.** 2007. Human blood-brain barrier disruption by retroviral-infected lymphocytes: role of myosin light chain kinase in endothelial tight-junction disorganization. J Immunol **179:**2576–2583. http://dx.doi.org/10.4049/jimmunol.179.4.2576.
7. **Chen CJ, Ou YC, Li JR, Chang CY, Pan HC, Lai CY, Liao SL, Raung SL, Chang CJ.** 2014. Infection of pericytes in vitro by Japanese encephalitis virus disrupts the integrity of the endothelial barrier. J Virol **88:**1150–1161. http://dx.doi.org/10.1128/JVI.02738-13.
8. **Chai Q, She R, Huang Y, Fu ZF.** 2015. Expression of neuronal CXCL10 induced by rabies virus infection initiates infiltration of inflammatory cells, production of chemokines and cytokines, and enhancement of blood-brain barrier permeability. J Virol **89:**870–876. http://dx.doi.org/10.1128/JVI.02154-14.
9. **Obermeier B, Daneman R, Ransohoff RM.** 2013. Development, maintenance and disruption of the blood-brain barrier. Nat Med **19:**1584–1596. http://dx.doi.org/10.1038/nm.3407.
10. **Arbour N, Day R, Newcombe J, Talbot PJ.** 2000. Neuroinvasion by human respiratory coronaviruses. J Virol **74:**8913–8921. http://dx.doi.org/10.1128/JVI.74.19.8913-8921.2000.
11. **Murray RS, Brown B, Brian D, Cabirac GF.** 1992. Detection of coronavirus RNA and antigen in multiple sclerosis brain. Ann Neurol **31:**525–533. http://dx.doi.org/10.1002/ana.410310511.
12. **Stewart JN, Mounir S, Talbot PJ.** 1992. Human coronavirus gene expression in the brains of multiple sclerosis patients. Virology **191:**502–505. http://dx.doi.org/10.1016/0042-6822(92)90220-J.
13. **Gu J, Gong E, Zhang B, Zheng J, Gao Z, Zhong Y, Zou W, Zhan J, Wang S, Xie Z, Zhuang H, Wu B, Zhong H, Shao H, Fang W, Gao D, Pei F, Li X, He Z, Xu D, Shi X, Anderson VM, Leong AS.** 2005. Multiple organ infection and the pathogenesis of SARS. J Exp Med **202:**415–424. http://dx.doi.org/10.1084/jem.20050828.
14. **Cowley TJ, Weiss SR.** 2010. Murine coronavirus neuropathogenesis: determinants of virulence. J Neurovirol **16:**427–434. http://dx.doi.org/10.1007/BF03210848.
15. **Virelizier JL, Dayan AD, Allison AC.** 1975. Neuropathological effects of persistent infection of mice by mouse hepatitis virus. Infect Immun **12:**1127–1140.
16. **Tardieu M, Goffinet A, Harmant-van Rijckevorsel G, Lyon G.** 1982. Ependymitis, leukoencephalitis, hydrocephalus, and thrombotic vasculitis following chronic infection by mouse hepatitis virus 3 (MHV3). Acta Neuropathol **58:**168–176. http://dx.doi.org/10.1007/BF00690797.
17. **Martin JP, Chen W, Koehren F, Pereira CA.** 1994. The virulence of mouse hepatitis virus 3, as evidenced by permissivity of cultured hepatic cells toward escaped mutants. Res Virol **145:**297–302. http://dx.doi.org/10.1016/S0923-2516(07)80034-3.
18. **Jacques A, Bleau C, Martin JP, Lamontagne L.** 2008. Intrahepatic endothelial and Kupffer cells involved in immunosuppressive cytokines and natural killer (NK)/NK T cell disorders in viral acute hepatitis. Clin Exp Immunol **152:**298–310. http://dx.doi.org/10.1111/j.1365-2249.2008.03628.x.
19. **Lavi E, Gilden DH, Highkin MK, Weiss SR.** 1986. The organ tropism of mouse hepatitis virus A59 in mice is dependent on dose and route of inoculation. Lab Anim Sci **36:**130–135.
20. **Netland J, Meyerholz DK, Moore S, Cassell M, Perlman S.** 2008. Severe acute respiratory syndrome coronavirus infection causes neuronal death in the absence of encephalitis in mice transgenic for human ACE2. J Virol **82:**7264–7275. http://dx.doi.org/10.1128/JVI.00737-08.
21. **Barnett EM, Perlman S.** 1993. The olfactory nerve and not the trigeminal nerve is the major site of CNS entry for mouse hepatitis virus, strain JHM. Virology **194:**185–191. http://dx.doi.org/10.1006/viro.1993.1248.

22. **Godfraind C, Havaux N, Holmes KV, Coutelier JP.** 1997. Role of virus receptor-bearing endothelial cells of the blood-brain barrier in preventing the spread of mouse hepatitis virus-A59 into the central nervous system. J Neurovirol **3:**428–434. http://dx.doi.org/10.3109/13550289709031188.
23. **Belouzard S, Millet JK, Licitra BN, Whittaker GR.** 2012. Mechanisms of coronavirus cell entry mediated by the viral spike protein. Viruses **4:**1011–1033. http://dx.doi.org/10.3390/v4061011.
24. **Joseph J, Kim R, Siebert K, Lublin FD, Offenbach C, Knobler RL.** 1995. Organ specific endothelial cell heterogeneity influences differential replication and cytopathogenicity of MHV-3 and MHV-4. Adv Exp Med Biol **380:**43–50. http://dx.doi.org/10.1007/978-1-4615-1899-0_6.
25. **Lavi E, Das Sarma J, Weiss SR.** 1999. Cellular reservoirs for coronavirus infection of the brain in beta2-microglobulin knockout mice. Pathobiology **67:**75–83. http://dx.doi.org/10.1159/000028054.
26. **Godfraind C, Coutelier JP.** 1998. Morphological analysis of mouse hepatitis virus A59-induced pathology with regard to viral receptor expression. Histol Histopathol **13:**181–199.
27. **Dupuy JM, Rodrigue D.** 1981. Heterogeneity in evolutive patterns of inbred mice infected with a cloned substrain of mouse hepatitis virus type 3. Intervirology **16:**114–117. http://dx.doi.org/10.1159/000149255.
28. **Phares TW, Kean RB, Mikheeva T, Hooper DC.** 2006. Regional differences in blood-brain barrier permeability changes and inflammation in the apathogenic clearance of virus from the central nervous system. J Immunol **176:**7666–7675. http://dx.doi.org/10.4049/jimmunol.176.12.7666.
29. **Tardieu M, Boespflug O, Barbé T.** 1986. Selective tropism of a neurotropic coronavirus for ependymal cells, neurons, and meningeal cells. J Virol **60:**574–582.
30. **Yen LF, Wei VC, Kuo EY, Lai TW.** 2013. Distinct patterns of cerebral extravasation by Evans blue and sodium fluorescein in rats. PLoS One **8:**e68595. http://dx.doi.org/10.1371/journal.pone.0068595.
31. **Gralinski LE, Ashley SL, Dixon SD, Spindler KR.** 2009. Mouse adenovirus type 1-induced breakdown of the blood-brain barrier. J Virol **83:**9398–9410. http://dx.doi.org/10.1128/JVI.00954-09.
32. **Watanabe T, Dohgu S, Takata F, Nishioku T, Nakashima A, Futagami K, Yamauchi A, Kataoka Y.** 2013. Paracellular barrier and tight junction protein expression in the immortalized brain endothelial cell lines bEND.3, bEND.5 and mouse brain endothelial cell 4. Biol Pharm Bull **36:**492–495. http://dx.doi.org/10.1248/bpb.b12-00915.
33. **Brown RC, Morris AP, O'Neil RG.** 2007. Tight junction protein expression and barrier properties of immortalized mouse brain microvessel endothelial cells. Brain Res **1130:**17–30. http://dx.doi.org/10.1016/j.brainres.2006.10.083.
34. **Jacques A, Bleau C, Turbide C, Beauchemin N, Lamontagne L.** 2009. Macrophage interleukin-6 and tumour necrosis factor-alpha are induced by coronavirus fixation to Toll-like receptor 2/heparan sulphate receptors but not carcinoembryonic cell adhesion antigen 1a. Immunology **128**(Suppl 1):e181–e192. http://dx.doi.org/10.1111/j.1365-2567.2008.02946.x.
35. **Fine M, Llaguno MC, Lariccia V, Lin MJ, Yaradanakul A, Hilgemann DW.** 2011. Massive endocytosis driven by lipidic forces originating in the outer plasmalemmal monolayer: a new approach to membrane recycling and lipid domains. J Gen Physiol **137:**137–154. http://dx.doi.org/10.1085/jgp.201010469.
36. **Daniels BP, Holman DW, Cruz-Orengo L, Jujjavarapu H, Durrant DM, Klein RS.** 2014. Viral pathogen-associated molecular patterns regulate blood-brain barrier integrity via competing innate cytokine signals. mBio **5**(5):e01476-14. http://dx.doi.org/10.1128/mBio.01476-14.
37. **Kraus J, Ling AK, Hamm S, Voigt K, Oschmann P, Engelhardt B.** 2004. Interferon-beta stabilizes barrier characteristics of brain endothelial cells in vitro. Ann Neurol **56:**192–205. http://dx.doi.org/10.1002/ana.20161.
38. **Mineta K, Yamamoto Y, Yamazaki Y, Tanaka H, Tada Y, Saito K, Tamura A, Igarashi M, Endo T, Takeuchi K, Tsukita S.** 2011. Predicted expansion of the claudin multigene family. FEBS Lett **585:**606–612. http://dx.doi.org/10.1016/j.febslet.2011.01.028.
39. **Nakamuta S, Endo H, Higashi Y, Kousaka A, Yamada H, Yano M, Kido H.** 2008. Human immunodeficiency virus type 1 gp120-mediated disruption of tight junction proteins by induction of proteasome-mediated degradation of zonula occludens-1 and -2 in human brain microvascular endothelial cells. J Neurovirol **14:**186–195. http://dx.doi.org/10.1080/13550280801993630.
40. **Eifart P, Ludwig K, Böttcher C, de Haan CA, Rottier PJ, Korte T, Herrmann AJ.** 2007. Role of endocytosis and low pH in murine hepatitis virus strain A59 cell entry. Virology **81:**10758–10768. http://dx.doi.org/10.1128/JVI.00725-07.
41. **Burkard C, Verheije MH, Wicht O, van Kasteren SI, van Kuppeveld FJ, Haagmans BL, Pelkmans L, Rottier PJ, Bosch BJ, de Haan CA.** 2014. Coronavirus cell entry occurs through the endo-/lysosomal pathway in a proteolysis-dependent manner. PLoS Pathog **10:**e1004502. http://dx.doi.org/10.1371/journal.ppat.1004502.
42. **Soong G, Reddy B, Sokol S, Adama R, Prince A.** 2004. TLR2 is mobilized into an apical lipid raft receptor complex to signal infection in airway epithelial cells. J Clin Invest **113:**1482–1489. http://dx.doi.org/10.1172/JCI200420773.
43. **Zhou H, Zhao J, Perlman S.** 2010. Autocrine interferon priming in macrophages but not dendritic cells results in enhanced cytokine and chemokine production after coronavirus infection. mBio **1**(4):e00219-10. http://dx.doi.org/10.1128/mBio.00219-10.
44. **Nagyoszi P, Wilhelm I, Farkas AE, Fazakas C, Dung NT, Hasko J, Krizbbai IA.** 2010. Expression and regulation of Toll-like receptors in cerebral endothelial cells. Neurochem Int **57:**556–564. http://dx.doi.org/10.1016/j.neuint.2010.07.002.
45. **Zhou J, Stohlman SA, Hinton DR, Marten NW.** 2003. Neutrophils promote mononuclear cell infiltration during viral-induced encephalitis. J Immunol **170:**3331–3336. http://dx.doi.org/10.4049/jimmunol.170.6.3331.
46. **Rose KM, Weiss SR.** 2009. Murine coronavirus cell type dependent interaction with the type I interferon response. Viruses **1:**689–712. http://dx.doi.org/10.3390/v1030689.
47. **Patkar C, Giaya K, Libraty DH.** 2013. Dengue virus type 2 modulates endothelial barrier function through CD73. Am J Trop Med Hyg **88:**89–94. http://dx.doi.org/10.4269/ajtmh.2012.12-0474.
48. **Vassão RC, Mello IG, Pereira CA.** 1994. Role of macrophages, interferon gamma and procoagulant activity in the resistance of genetic heterogeneous mouse populations to mouse hepatitis virus infection. Arch Virol **137:**277–288. http://dx.doi.org/10.1007/BF01309475.
49. **Cabirac GF, Murray RS, McLaughlin LB, Skolnick DM, Hogue B, Dorovini-Zis K, Didier PJ.** 1995. In vitro interaction of coronaviruses with primate and human brain microvascular endothelial cells. Adv Exp Med Biol **380:**79–88. http://dx.doi.org/10.1007/978-1-4615-1899-0_11.
50. **Mazaleuskaya L, Veltrop R, Ikpeze N, Martin-Garcia J, Navas-Martin S.** 2012. Protective role of Toll-like receptor 3-induced type I interferon in murine coronavirus infection of macrophages. Viruses **4:**901–923. http://dx.doi.org/10.3390/v4050901.